On the Development of a New Master Device Used for Medical Tasks

Houssem Saafi, Med Amine Laribi, Said Zeghloul, Marc Arsicault

On the Development of a New Master Device Used for Medical Tasks

Houssem Saafi
Mechanical Laboratory of Sousse National Engineering,
School of Sousse,
University of Sousse,
Sousse 4054, Tunisia
e-mail: houssem.saafi@gmail.com

Med Amine Laribi[1]
Department GMSC,
Pprime Institute,
CNRS—University of Poitiers-ENSMA,
UPR 3346,
86962 Futuroscope Chasseneuil Cedex, France
e-mail: med.amine.laribi@univ-poitiers.fr

Said Zeghloul
Department GMSC,
Pprime Institute,
CNRS—University of Poitiers-ENSMA,
UPR 3346,
86962 Futuroscope Chasseneuil Cedex, France
e-mail: said.zeghloul@univ-poitiers.fr

Marc Arsicault
Department GMSC,
Pprime Institute,
CNRS—University of Poitiers-ENSMA,
UPR 3346,
86962 Futuroscope Chasseneuil Cedex, France
e-mail: marc.arsicault@univ-poitiers.fr

This paper discusses the design of a new spherical parallel manipulator (SPM), which is used as a master device for medical tasks. This device is obtained by changing the kinematics of a classic SPM to eliminate the singularity from the device's useful workspace. The kinematic models of the new device are studied. The geometric parameters of the new device are optimized to eliminate the singularity. A prototype of the new master device is presented. Experiments are carried out using the device which allowed the control of a surgical robot.

1 Introduction

Master devices have been introduced in recent years to control the motion of either virtual objects or slave robots. Those devices are designed for many applications such as gaming [1], virtual reality [2,3], research [4,5], or medicine [6,7].

Many master devices have been developed as a part of surgical teleoperation systems. Van den Bedem et al. [7] proposed a master device with a four degrees-of-freedom (DOF) serial architecture, which was developed to control the *SOFIE surgical robot*. Tobergte et al. [6] proposed a 7DOF hybrid master device called 7 Sigma. This device was designed to control the *Miro surgical robot* [5].

In a previous work [8], a master device was designed to control a surgical robot and apply interaction forces to the manipulator (Fig. 1). However, due to the presence of the singularity, the developed master device did not meet the requirements. Bonev and Gosselin [9] studied the workspace and singularity of spherical parallel manipulators. In a previous work, we have proposed solutions based on the redundancy of sensors [10,11] and actuators [12] to solve the problems of the singularity. Those problems are the amplification of error of the resolution of the forward kinematic model and the amplification of the actuated joint torques. However, the addition of the actuator on the moving platform has increased the weight of the structure and decreased the force range.

In this paper, we propose a second alternative. The proposed structure by Chaker et al. [8] has several advantages. Indeed, the interface provides the desired degrees-of-freedom, which are three pure rotations. In addition, it has good mechanical properties such as stiffness, precision, and lightness. However, this structure has a major limitation, which is the presence of the parallel singularity. The singularity depends on the kinematics of the robot. Changing the kinematic of one leg of the master device can solve these singularity problems. Birglen et al. [4] changed the kinematics of a leg of a spherical parallel manipulator (SPM), called *SHADE*, to solve an interference problem. The proposed solution is inspired from Birglen robot. The goal of this work is to propose a master device without presence of singularities, without major change of the mechanical structure and with the same mobility as the first master device.

This paper is organized as follows: The kinematics of the new master device is presented in Sec. 2. In Sec. 3, an evaluation of the new structure is established. An optimization of the geometric parameters of the new master device is made in Sec. 4 to eliminate the singularity from the useful workspace. In Sec. 5, the forward kinematic model of the device is evaluated. The haptic control model is presented in Sec. 6.

2 Kinematics of the New Master Device

The medical application requires a mechanism having four degrees-of-freedom, which are three pure rotations, and one translation. The spherical architecture gives three pure rotations, which can be described by the Euler angles ψ, θ and φ. ψ and θ are called tilt angles and φ is the self-rotation angle.

The new architecture is shown in Fig. 2. This architecture is obtained by replacing the (RRR) kinematics of the leg A by the (URU) kinematics (R for revolute, U for universal). The kinematics of the new leg A is shown in Fig. 3. The new interface has the same mobility as the classical SPM, which are three pure rotations.

For legs B and C, the kinematic model is given by Eq. (1) and obtained by differentiating the equation $Z_{2k} \cdot Z_{3k} = \cos(\beta)$ for $k = B$ and C. Where ω is the angular velocity of the moving platform

$$\begin{cases} Z_{1B} \times Z_{2B} \cdot Z_{3B}\dot{\theta}_{1B} = Z_{2B} \times Z_{3B} \cdot \omega \\ Z_{1C} \times Z_{2C} \cdot Z_{3C}\dot{\theta}_{1C} = Z_{2C} \times Z_{3C} \cdot \omega \end{cases} \quad (1)$$

For the A leg, we can write the following equation:

$$\omega = \dot{\theta}_{1A} \cdot Z_{1A} + \dot{\theta}_{2A} \cdot Z_{2A} + \dot{\theta}_{3A} \cdot Z_{3A} + \dot{\theta}_{4A} \cdot Z_{4A} + \dot{\theta}_{5A} \cdot Z_{5A} \quad (2)$$

Only the angle $\dot{\theta}_{1A}$ is active. To eliminate passive angular velocities $\dot{\theta}_{2A}$, $\dot{\theta}_{3A}$, $\dot{\theta}_{4A}$, and $\dot{\theta}_{5A}$, we multiply Eq. (2) by a vector perpendicular to all leg A axes except the Z_{1A} axis. This vector is defined as

$$V_r = Z_{4A} \times Z_{5A} \quad (3)$$

Equation (2) becomes

$$Z_{4A} \times Z_{5A} \cdot Z_{1A}\dot{\theta}_{1A} = Z_{4A} \times Z_{5A} \cdot \omega \quad (4)$$

[1]Corresponding author.

Contributed by the Mechanisms and Robotics Committee of ASME for publication in the Journal of Mechanisms and Robotics. Manuscript received July 13, 2017; final manuscript received February 28, 2018; published online April 11, 2018. Assoc. Editor: Clement Gosselin.

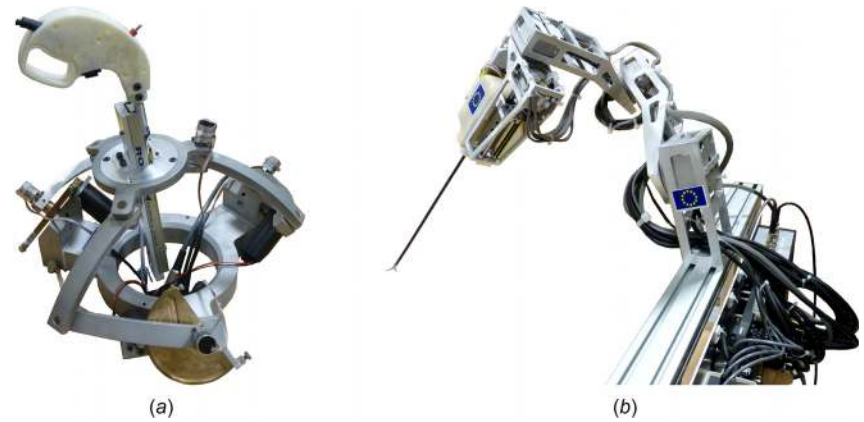

Fig. 1 Master device (*a*) and a surgical robot (*b*) of a medical tele-operation system

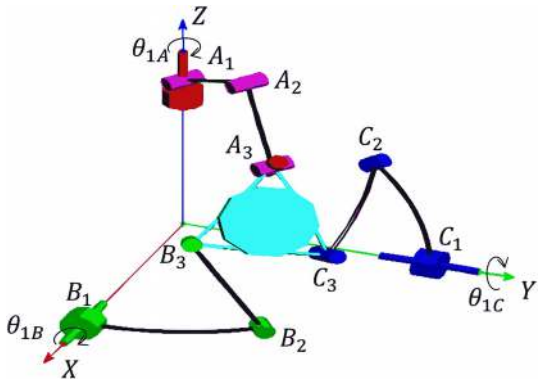

Fig. 2 New kinematics of the master device

The kinematic model is as follows:

$$\begin{cases} Z_{4A} \times Z_{5A} \cdot Z_{1A}\dot{\theta}_{1A} = Z_{4A} \times Z_{5A} \cdot \omega \\ Z_{1B} \times Z_{2B} \cdot Z_{3B}\dot{\theta}_{1B} = Z_{2B} \times Z_{3B} \cdot \omega \\ Z_{1C} \times Z_{2C} \cdot Z_{3C}\dot{\theta}_{1C} = Z_{2C} \times Z_{3C} \cdot \omega \end{cases} \tag{5}$$

which can be written as

$$\mathbf{A} \cdot \boldsymbol{\omega} = \mathbf{B} \cdot \dot{\boldsymbol{\Theta}} \tag{6}$$

where

$$\dot{\boldsymbol{\Theta}} = \begin{bmatrix} \dot{\theta}_{1A} \\ \dot{\theta}_{1B} \\ \dot{\theta}_{1C} \end{bmatrix} \tag{7}$$

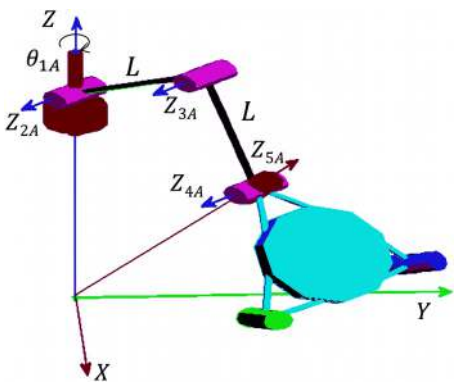

Fig. 3 Kinematics of the leg A

$$\omega = \begin{bmatrix} \dot{\theta} \cdot \cos(\psi) + \dot{\varphi} \cdot \sin(\theta) \cdot \sin(\psi) \\ \dot{\theta} \cdot \sin(\psi) - \dot{\varphi} \cdot \sin(\theta) \cdot \cos(\psi) \\ \dot{\psi} + \dot{\varphi} \cdot \cos(\theta) \end{bmatrix} \tag{8}$$

$$\mathbf{A} = \begin{bmatrix} (\mathbf{Z}_{5A} \times \mathbf{Z}_{4A})^{\mathrm{T}} \\ (\mathbf{Z}_{3B} \times \mathbf{Z}_{2B})^{\mathrm{T}} \\ (\mathbf{Z}_{3C} \times \mathbf{Z}_{2C})^{\mathrm{T}} \end{bmatrix} \tag{9}$$

$$\mathbf{B} = \begin{bmatrix} \mathbf{Z}_{1A} \cdot (\mathbf{Z}_{4A} \times \mathbf{Z}_{5A}) & 0 & 0 \\ 0 & \mathbf{Z}_{1B} \cdot (\mathbf{Z}_{2B} \times \mathbf{Z}_{3B}) & 0 \\ 0 & 0 & \mathbf{Z}_{1C} \cdot (\mathbf{Z}_{2C} \times \mathbf{Z}_{3C}) \end{bmatrix} \tag{10}$$

where ω is the angular velocity of the moving platform and $\dot{\boldsymbol{\Theta}}$ is the angular velocity of the active joints. The matrices $\mathbf{A}$ and $\mathbf{B}$ are the parallel and serial parts of the Jacobian matrix, respectively.

The Jacobian matrix is

$$\mathbf{J} = \mathbf{A}^{-1}\mathbf{B} \tag{11}$$

3 Kinematic Evaluation of the New Structure

The modification of the architecture of the SPM is made to eliminate the singularity from its workspace. In this section, we evaluate the presence of the singularity for each working mode of the new SPM. The working modes are the solutions of the IKM. The IKM of the new SPM has eight solutions similarly to the classic SPM [13]. Only one configuration of the leg A is considered, so, the new SPM has only four working modes presented in Fig. 4.

The working modes are compared to select the less singular one. To evaluate the new SPM, we use the dexterity as a criterion. The dexterity $\eta(\mathrm{J})$ is given by the inverse of the condition number of the Jacobian matrix as follows:

$$\eta(J) = \frac{1}{||J^{-1}|| \cdot ||J||} \tag{12}$$

This evaluation is performed for each working mode (Fig. 4). The dexterity distribution is evaluated for a useful workspace in the (ψ, θ) plane for φ equals 0 deg, 50 deg, and −50 deg. The useful workspace is the workspace of the minimally invasive surgery studied in Ref. [14] (Fig. 5).

We propose to calculate the minimum distance between the singular area and the center of the useful workspace defined by the point O_0=(ψ, θ) = (135 deg, 54 deg) (Fig. 6).

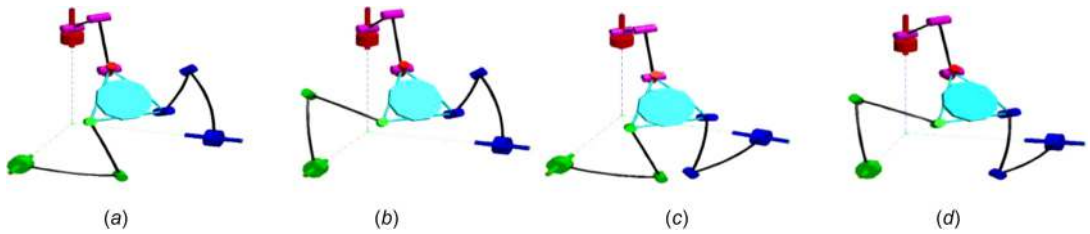

Fig. 4 Working modes of the new SPM: (*a*) working mode 1, (*b*) working mode 2, (*c*) working mode 3, and (*d*) working mode 4

This distance is calculated as follows:

$$r_{\min} = \min(r_i) = \min\left(\sqrt{(\psi_i - \psi_0)^2 + (\theta_i - \theta_0)^2}\right) \quad (13)$$

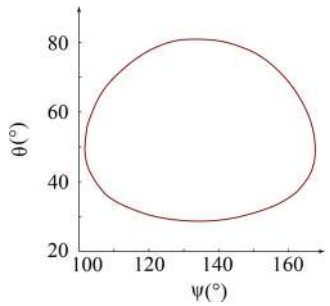

Fig. 5 Useful workspace in the plane (ψ, θ)

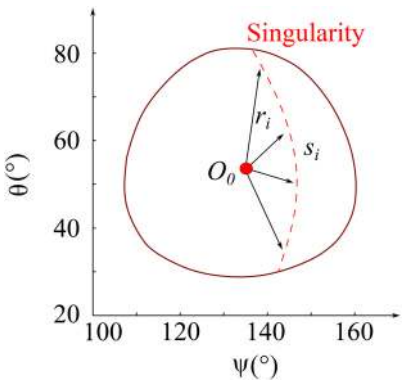

Fig. 6 Minimum distance identification

The SPM is considered in a singular configuration if the value of the dexterity is less than 0.02. Figure 7 shows the evolution of $r_{\min}$ according to the self-rotation φ. We observe that for working mode 2 the singular areas are close to the border of the workspace. Consequently, we chose mode 2 as the working mode.

The symmetry of the architecture of mode 2 has led to a symmetrical kinematic behaviors. Because of this symmetry, the study in the next paragraph will focus only on the self-rotation between 0 deg and 50 deg.

In addition to the presence of the singularity for $\varphi = -50$ deg and $\varphi = 50$ deg, the size of the workspace does not match the useful workspace (Fig. 8).

This study shows that the modification decreased the presence of the singularity of the workspace in comparison with the classic

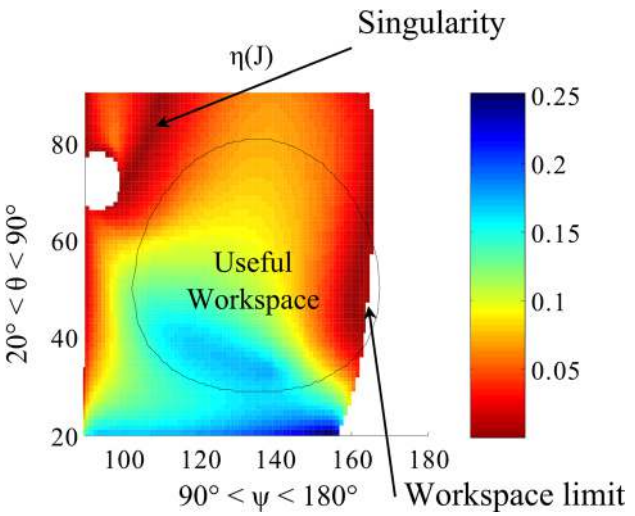

Fig. 8 Limitation of the new SPM

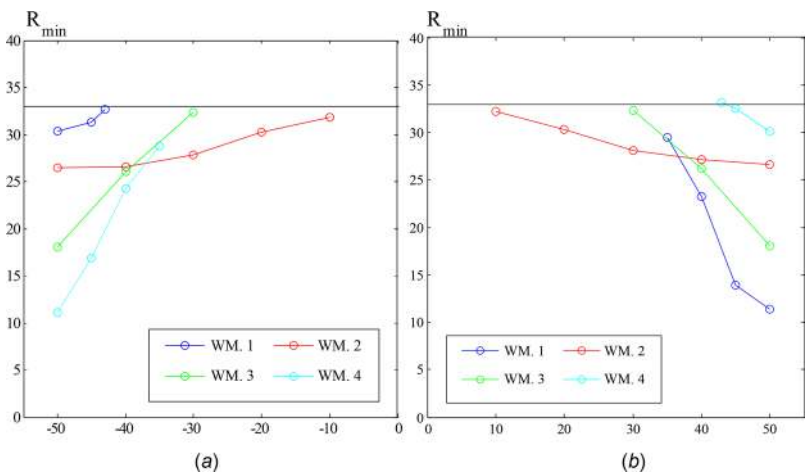

Fig. 7 $r_{\min}$ evolution for each working mode

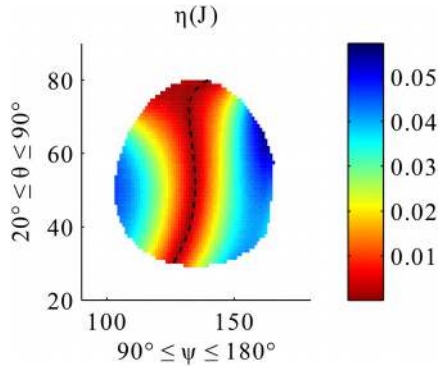

Fig. 9 Dexterity distribution of the classic SPM $\varphi = 50$ deg

SPM. The dexterity distribution of the classical SPM is shown in Fig. 9.

To increase the size of the workspace and eliminate the presence of the singularity for the new SPM, we propose to optimize its geometrical parameters in Sec. 4.

4 Optimization of the New Spherical Parallel Manipulator

Dexterity is considered as the optimization criterion. By analyzing the Jacobian matrix of the new SPM, we can observe that the geometric parameters of the leg A have no influence on its kinematic behavior. For this reason, only the geometrical parameters of leg B and C (α, β, γ) are optimized.

The design vector of the optimization process is

$$I = \begin{bmatrix} \alpha \\ \beta \\ \gamma \end{bmatrix} \tag{14}$$

The purpose of the optimization process is not only to eliminate the singularity from the workspace, but also to increase the workspace and to reach the useful workspace for φ equal to 50 deg.

Only the workspace boundary is considered. Indeed, the border is discretized into 100 points (Fig. 10). For each point, the optimization algorithm verifies that the conditions of the workspace are met and verifies the condition number of the Jacobian matrix. This check is made for two self-rotation values, $\varphi = 0$ deg and $\varphi = 50$ deg.

The optimization process can be defined as follows:

$$\begin{aligned} \underset{I}{\text{minimize}} \quad & F(I) = \sum_{i}^{N} (\kappa(I, P_i, \varphi = 0) + \sum_{i}^{N} (\kappa(I, P_i, \varphi = 50) \\ \text{subject to} \quad & (1) \quad \kappa(I, P_i) < \kappa_{\max}. \\ & (2) \quad x_{\text{lo}} \leq x \leq x_{\text{up}}, x \in \{\alpha, \beta, \gamma\}. \\ & (3) \quad CD_j(\alpha, \beta, \gamma, \psi, \theta, \phi) : \frac{C_j^2}{A_j^2 + B_j^2} \leq 1 \quad \text{for } j = 1, 2 \end{aligned}$$

Where $F(I)$ is the objective function defined as the sum of the condition number of the Jacobian matrix for $\varphi = 0$ deg and $\varphi = 50$ deg. By minimizing $F(I)$, we maximize the dexterity distribution.

x_{lo} and x_{up} are the lower limits and upper limits of the geometric parameters. These parameters are defined in Table 1. $\kappa_{\max}$ is the maximum value of the condition number allowed in the optimization process to consider that the SPM is not in a singular configuration. This value is equal to 25.

The optimization method considered for this problem is a global method based on genetic algorithms due to its robustness and simplicity. Initially, the algorithm generates 500 samples of the design parameters. Then the three genetic operations (reproduction, crossover and mutation) are performed to produce a new generation. These procedures are repeated until reaching the maximum number of generations or satisfying the required accuracy.

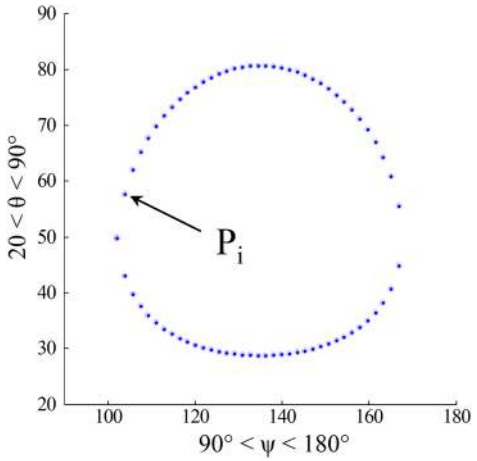

Fig. 10 Discretized border of the useful workspace

Table 1 The lower and upper limits of geometrical parameters

	α	β	γ
x_{inf}	35 deg	30 deg	16 deg
x_{sup}	50 deg	45 deg	20 deg

The optimal geometrical parameters are

$$I_{\text{op}} = \begin{bmatrix} \alpha_{\text{op}} \\ \beta_{\text{op}} \\ \gamma_{\text{op}} \end{bmatrix} = \begin{bmatrix} 49.5 \text{ deg} \\ 39.1 \text{ deg} \\ 16.1 \text{ deg} \end{bmatrix} \tag{15}$$

The size of the new leg is defined by the parameters L. It is calculated using the following expression:

$$L = R \sin\left(\frac{\theta_{2A}^{\max}}{2}\right) \tag{16}$$

Where R is the radius of the new SPM and $\theta_{2A}^{\max} = \theta^{\max} + \delta + \gamma$ is the maximum angle between Z_{1A} and Z_{5A}. δ is a security angle to avoid the serial singularity of the leg A. It is equal to 2 deg.

The optimal SPM is presented in Fig. 11.

The dexterity distributions of the optimal SPM for $\varphi = 0$ deg, $\varphi = 50$ deg, and $\varphi = -50$ deg are presented in Fig. 12. We observe that the SPM workspace covers the useful workspace for φ between -50 deg and 50 deg, which means that the new SPM is able to reach all orientations to perform the surgical tasks. In addition, we observe that the workspace is singularity-free for φ between -50 deg and 50 deg.

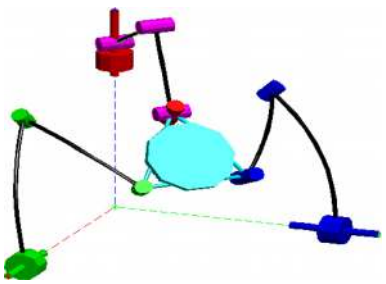

Fig. 11 Optimal new SPM

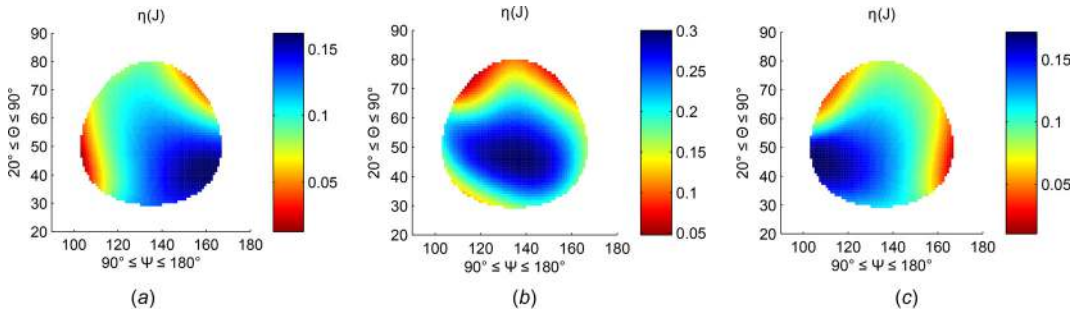

Fig. 12 Dexterity distributions for the optimal SPM: (*a*) $\varphi = -50$ deg, (*b*) $\varphi = 0$ deg, and (*c*) $\varphi = 50$ deg

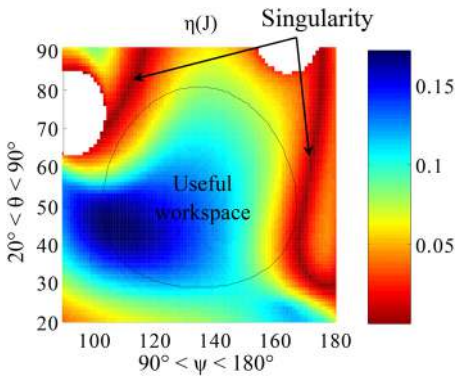

Fig. 13 Dexterity distribution of the optimal SPM for $\varphi = 50$ deg

Figure 13 shows the area of singularity for the optimal SPM for $\varphi = 50$ deg. We can observe that the singularity is outside the useful workspace.

The promising results obtained in this section allowed the development of a prototype of this new interface. The developed prototype is presented in Fig. 14.

Most mechanical parts of the classical device were kept. Only leg A and the moving platform are changed. This device is designed to control the surgical robot. The forward kinematic model must be solved with good accuracy in real time. However, the forward kinematics of parallel manipulators is complex [15–17]. The forward kinematic model of the new device is equivalent to that of other mechanisms presented in previous works [10,11]. This model was solved using a technique based on the input/output equations of a spherical four-bar mechanism [18–20].

Fig. 14 Prototype of the new device

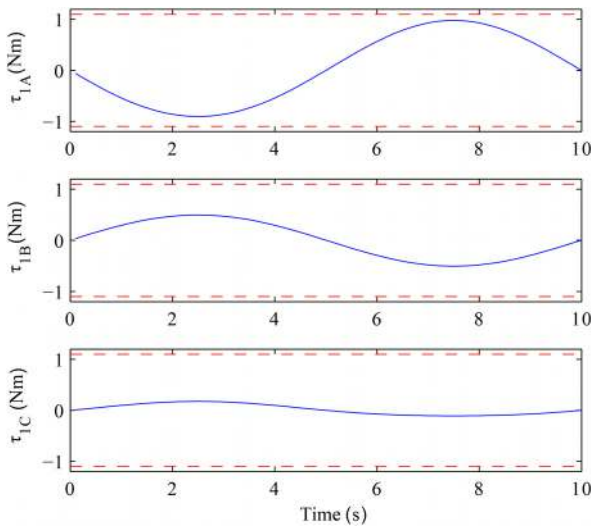

Fig. 15 Actuated joint torques

5 Haptic Control Model

5.1 Actuators Sizing of the New Device. In this paragraph, we discuss the choice of the actuators. A study using SIMMECHANICS was carried out to identify the required actuated joint torques. SIMMECHANICS library blocks are used to build the model. The inputs of the model are the joint motions and the force applied by the haptic device. The outputs are the actuated joint torques. The inverse dynamic model is called in SIMULINK to determine the actuated joint torques. The applied force is equal to 5 N [7]. Multiple simulations were carried out to identify the actuated joint torques limits. The force was applied in many directions and the orientation of the moving platform was varied. After this study, the chosen actuators are DC motors that give about $1.1\,\mathrm{N}\cdot\mathrm{m}$ with the reducers. Figure 15 shows an example of the actuated joint torques. For this example, the moving platform self-rotation was varied around 50 deg for $(\psi, \theta) = (135\,\mathrm{deg}, 54\,\mathrm{deg})$ (Fig. 16) and the

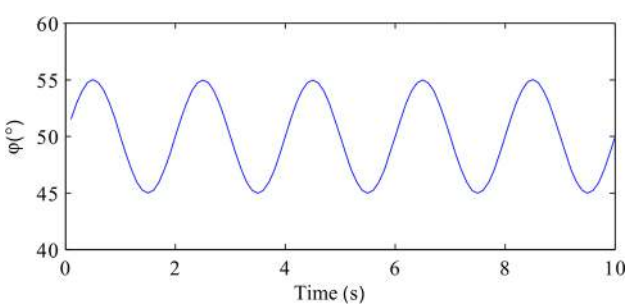

Fig. 16 Self-rotation (φ) evolution for (ψ, θ)=(135 deg, 54 deg)

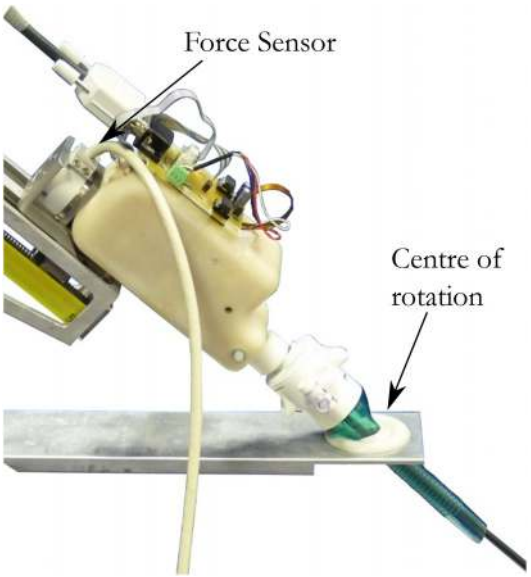

Fig. 17 Force sensor installed on the slave robot

applied force was varied sinusoidally between $-5N$ and $5N$. We can see that the actuated joint torques stay with the torques limits.

5.2 Haptic Control Model. The force sensor measures the force applied on the surgical robot (Fig. 17). Then, the actuated torques required to reproduce the force to the user are calculated using the following equation:

$$\boldsymbol{\tau} = J^T \mathbf{T} + \boldsymbol{\tau}_s \tag{17}$$

where $\boldsymbol{\tau}$ is the actuated joint torque vector, $\mathbf{T}$ is the end effector reference torque vector, and $\boldsymbol{\tau}_s$ is the static compensation torque vector. The Jacobian matrix is expressed in Sec. 2. The vector T will be given by the force sensor installed on the slave surgical robot (Fig. 17).

The force sensor is being calibrated; therefore, experiments of the haptic control will be presented in future work.

6 Conclusion

In this paper, a new haptic device is developed. This device is obtained by replacing the architecture of one leg of a classical spherical parallel manipulator. The device is developed to solve problems of the parallel singularity of the classical spherical parallel manipulator. A kinematic evaluation of the new device is carried out and shows the presence of a small singular area in the border of the workspace. In order to completely eliminate the singularity from the workspace, the geometric parameters of the new device are optimized. The forward kinematic model is solved in real time with good accuracy, which allowed the control of the surgical slave robot using the new device. The haptic control model is developed and will be used once the force sensor is calibrated.

Acknowledgment

This research is supported by ROBOTEX, the French national network of robotics platforms (No. ANR-10-EQPX-44-01). This research is supported by the region Nouvelle-Aquitaine (program HABISAN 2015-2020) with the financial participation of the European Union (FEDER/ERDF, European Regional Development Fund).

References

[1] Park, W., Kim, L., Cho, H., and Park, S., 2009, "Design of Haptic Interface for Brickout Game," IEEE International Workshop on Haptic Audio visual Environments and Games (HAVE), Lecco, Italy, Nov. 7–8, pp. 64–68.
[2] Gosselin, F., Jouan, T., Brisset, J., and Andriot, C., 2005, "Design of a Wearable Haptic Interface for Precise Finger Interactions in Large Virtual Environments," Eurohaptics Conference, 2005 and Symposium on Haptic Interfaces for Virtual Environment and Teleoperator Systems, Pisa, Italy, Mar. 18–20, pp. 202–207.
[3] Ma, A., and Payandeh, S., 2008, "Analysis and Experimentation of a 4-DOF Haptic Device," Symposium on Haptic Interfaces for Virtual Environment and Teleoperator Systems (HAPTICS), Reno, NE, Mar. 13–14, pp. 351–356.
[4] Birglen, L., Gosselin, C., Pouliot, N., Monsarrat, B., and Laliberté, T., 2002, "Shade, a New 3-DOF Haptic Device," IEEE Trans. Rob. Autom., **18**(2), pp. 166–175.
[5] Hagn, U., Konietschke, R., Tobergte, A., Nickl, M., Jörg, S., Kübler, B., Passig, G., Gröger, M., Fröhlich, F., Seibold, U., Le-Tien, L., Albu-Schäffer, A., Nothhelfer, A., Hacker, F., Grebenstein, M., and Hirzinger, G., 2010, "DLR MiroSurge: A Versatile System for Research in Endoscopic Telesurgery," Int. J. Comput. Assisted Radiol. Surg., **5**(2), pp. 183–193.
[6] Tobergte, A., Helmer, P., Hagn, U., Rouiller, P., Thielmann, S., Grange, S., Albu-Schaffer, A., Conti, F., and Hirzinger, G., 2011, "The Sigma. 7 Haptic Interface for Mirosurge: A New Bi-Manual Surgical Console," IEEE/RSJ International Conference on Intelligent Robots and Systems (IROS), San Francisco, CA, Sept. 25–30, pp. 3023–3030.
[7] Van den Bedem, L., Hendrix, R., Rosielle, N., Steinbuch, M., and Nijmeijer, H., 2009, "Design of a Minimally Invasive Surgical Teleoperated Master-Slave System With Haptic Feedback," International Conference on Mechatronics and Automation (ICMA), Changchun, China, Aug. 9–12, pp. 60–65.
[8] Chaker, A., Mlika, A., Laribi, M. A., Romdhane, L., and Zeghloul, S., 2012, "Synthesis of Spherical Parallel Manipulator for Dexterous Medical Task," Front. Mech. Eng., **7**(2), pp. 150–162.
[9] Bonev, I. A., and Gosselin, C. M., 2006, "Analytical Determination of the Workspace of Symmetrical Spherical Parallel Mechanisms," IEEE Trans. Rob., **22**(5), pp. 1011–1017.
[10] Saafi, H., Laribi, M. A., and Zeghloul, S., 2015, "Forward Kinematic Model Improvement of a Spherical Parallel Manipulator Using an Extra Sensor," Mech. Mach. Theory, **91**, pp. 102–119.
[11] Saafi, H., Laribi, M. A., and Zeghloul, S., 2014, "Improvement of the Direct Kinematic Model of a Haptic Device for Medical Application in Real Time Using an Extra Sensor," IEEE/RSJ International Conference on Intelligent Robots and Systems (IROS), Chicago, IL, Sept. 14–18, pp. 1697–1702.
[12] Saafi, H., Laribi, M. A., and Zeghloul, S., 2015, "Redundantly Actuated 3-RRR Spherical Parallel Manipulator Used as a Haptic Device: Improving Dexterity and Eliminating Singularity," Robotica, **33**(5), pp. 1113–1130.
[13] Bonev, I. A., and Damien Chablat, P. W., 2006, "Working and Assembly Modes of the Agile Eye," IEEE International Conference on Robotics and Automation (ICRA), Orlando, FL, May 15–19, pp. 2317–2322.
[14] Laribi, M., Riviere, T., Arsicault, M., and Zeghloul, S., 2012, "A Design of Slave Surgical Robot Based on Motion Capture," IEEE International Conference on Robotics and Biomimetics (ROBIO), Guangzhou, China, Dec. 11–14, pp. 600–605.
[15] Gosselin, C. M., and Merlet, J.-P., 1994, "The Direct Kinematics of Planar Parallel Manipulators: Special Architectures and Number of Solutions," Mech. Mach. Theory, **29**(8), pp. 1083–1097.
[16] Merlet, J. P., 1993, "Direct Kinematics of Parallel Manipulators," IEEE Trans. Rob. Autom., **9**(6), pp. 842–846.
[17] Gosselin, C. M., Sefrioui, J., and Richard, M. J., 1994, "On the Direct Kinematics of Spherical Three-Degree-of-Freedom Parallel Manipulators of General Architecture," ASME J. Mech. Des., **116**(2), pp. 594–598.
[18] Bai, S., Hansen, M. R., and Angeles, J., 2009, "A Robust Forward-Displacement Analysis of Spherical Parallel Robots," Mech. Mach. Theory, **44**(12), pp. 2204–2216.
[19] Bai, S., and Hansen, M. R., 2008, "Forward Kinematics of Spherical Parallel Manipulators With Revolute Joints," IEEE/ASME International Conference on Advanced Intelligent Mechatronics (AIM), Xian, China, July 2–5, pp. 522–527.
[20] Vertechy, R., and Parenti-Castelli, V., 2008, "Robust, Fast and Accurate Solution of the Direct Position Analysis of Parallel Manipulators by Using Extra-Sensors," *Parallel Manipulators, Towards New Applications*, H. Wu, ed., InTech, Rijeka, Croatia.